Coordinate Transformation Uncertainty Analysis in Large-Scale Metrology

Yu Ren, Jiarui Lin, Jigui Zhu, Bo Sun, and Shenghua Ye

***Abstract*— 3-D coordinate transformation, which is based on aligning two sets of common reference points, is frequently applied in large-scale combined measurement to unify coordinate frames and tie individual measurement systems together. However, it introduces uncertainty into the final measurement results. This uncertainty must be quantified to make the results complete. This paper presents a novel approach to the uncertainty analysis of 3-D coordinate transformation based on the weighted total least squares adjustment. This approach takes full account of the uncertainty characteristics of measuring instruments and is simple in calculation. In this approach, the transformation uncertainty of a point in a world frame is analyzed carefully. The simulations show that the transformation uncertainty has a distribution of concentric ellipsoids and is affected by the measurement uncertainties and layout of common points. Besides, strategies for minimizing transformation uncertainty are recommended. The experimental results from a laser tracker prove that this proposed approach is valid under normal instrument operating conditions and that these strategies are feasible and efficient.**

***Index Terms*— Coordinate transformation, error analysis, large-scale metrology, position measurement, sensor fusion, uncertainty.**

I. Introduction

LARGE-SCALE 3-D coordinate measurement has become routine in industries such as giant antenna, aircraft, and ship construction. Since objects are usually large in size and rich with obstructions, many on-site measurement tasks require a combination of multiple measuring instruments. These instruments are tied together by 3-D coordinate transformation, which is based on aligning two sets of common reference points [1]–[3]. Any 3-D coordinate transformation method introduces uncertainty into the measurement results. This uncertainty must be quantified to ensure accurate and precise representation of its effects on the final measurement results. Moreover, it must be minimized with appropriate measurement configurations in on-site measurement tasks.

The importance of uncertainty estimation in 3-D coordinate transformation has been recognized in precision measurement. Yan and Menq [4] constructed a sensitivity matrix to link the coordinate transformation uncertainty and points' geometric errors. However, this approach assumes that a deterministic surface adequately representing the measured points can be easily constructed, which may not always be available. Che and Ni [5] proposed a coordinate transformation uncertainty assessment approach based on constrained optimization. This approach can be used for nonorthogonal coordinates. However, it is computationally complex, since higher derivatives of the objective function are necessary to propagate uncertainty. In addition, and importantly, the aforementioned approaches are studied based on the coordinate measuring machine, so they assume that a point's measurement uncertainty conforms nicely to the x-, y-, and z-axis representations ($\sigma_{xy} = \sigma_{yz} = \sigma_{zx}$).

Unfortunately, 3-D coordinate transformation uncertainty estimation has received less attention in large-scale metrology. Owing to the popularization of nonorthogonal coordinate measurement systems, such as theodolite, laser tracker, and iGPS, measurement uncertainty no longer conforms to the x-, y-, and z-axis representations [6]–[9]. Therefore, the aforementioned approaches cannot be adopted directly, and new estimation methods must consider the error characteristics of each system. The unified spatial metrology network (USMN), which combines measurements from multiple systems into a network complete with measurement uncertainty, was suggested in [3] and has been applied in commercial software spatial analyzer [10]. Since USMN is based on the Monte Carlo (MC) simulation, it can handle all the recognized sources of uncertainty; however, it is computationally more expensive than analytical methods [11]. In addition, current studies have focused only on quantifying the transformation uncertainty, but have not involved addition optimization around 3-D coordinate transformation process, such as optimization of common-point layout, instrument type, and placement.

This paper develops a novel 3-D coordinate transformation uncertainty estimation approach based on weighted total least squares (WTLS) adjustment, and analyzes the distribution of transformation uncertainty and its influencing factors. The aim is to recommend optimized strategies for minimizing transformation uncertainty in addition to quantifying it.

II. 3-D Coordinate Transformation Model

3-D coordinate transformation is based on aligning two sets of common points, and

$$\begin{bmatrix} x \\ y \\ z \end{bmatrix}_W = k\mathbf{R} \begin{bmatrix} x \\ y \\ z \end{bmatrix}_M + \mathbf{T} \tag{1}$$

Manuscript received September 22, 2014; revised November 23, 2014; accepted December 23, 2014. Date of publication February 27, 2015; date of current version August 7, 2015. This work was supported in part by the National Natural Science Foundation of China under Grant 51305297 and Grant 51225505 and in part by the Specialized Research Fund for the Doctoral Program of Higher Education under Grant 20130032120067. The Associate Editor coordinating the review process was Dr. Ruqiang Yan.

The authors are with the State Key Laboratory of Precision Measuring Technology and Instruments, Tianjin University, Tianjin 300072, China (e-mail: linjr@tju.edu.cn).

Color versions of one or more of the figures in this paper are available online at http://ieeexplore.ieee.org.

Digital Object Identifier 10.1109/TIM.2015.2403151

where the subscript W means the points in world coordinate frame $\{W\}$ and the subscript M means the corresponding points in measuring coordinate frame $\{M\}$. $\mathbf{R}$ is the rotation matrix from $\{M\}$ to $\{W\}$ and a function of the three rotation angles α, β, and γ

$$\mathbf{R} = \begin{bmatrix} \cos\alpha\cos\beta & \sin\alpha\cos\beta & -\sin\beta \\ \cos\alpha\sin\beta\sin\gamma - \sin\alpha\cos\gamma & \sin\alpha\sin\beta\sin\gamma + \cos\alpha\cos\gamma & \cos\beta\sin\gamma \\ \cos\alpha\sin\beta\cos\gamma + \sin\alpha\sin\gamma & \sin\alpha\sin\beta\cos\gamma - \cos\alpha\sin\gamma & \cos\beta\cos\gamma \end{bmatrix}. \tag{2}$$

$\mathbf{T}$ is the translation vector given by $\mathbf{T} = [\Delta x \ \Delta y \ \Delta z]^T$ and k is the scale factor.

Equation (2) shows the nonlinear structure of matrix $\mathbf{R}$. If the transformation parameters are estimated by nonconstrained optimization or constrained optimization method, higher derivatives of the objective function are necessary to compute their uncertainties, resulting in excessive calculation [12]. In surveying and geodesy, matrix $\mathbf{R}$ is usually linearized based on small rotation angles to simplify solution. Thus a linear model, the Bursa–Wolf model [13], [14], is adopted. In addition, Zeng and Tao [15] show that the error of rotation angle introduced by this model is less than 10^{-3} arc s, when rotation angle is within 2 arc s.

To satisfy rotation angles of any magnitude, an intermediate coordinate frame $\{M1\}$ is introduced between $\{M\}$ and $\{W\}$; in other words, the transformation between $\{M\}$ and $\{W\}$ is divided into two steps by $\{M1\}$ as in (3). $\{M1\}$ is a rigid rotation of $\{M\}$ as in (3a), which is calculated by 3-2-1 nesting method [3], [5]. Then the transformation between $\{M1\}$ and $\{W\}$ satisfies the Bursa–Wolf model, as shown in (3b). In addition, the price paid (in the uncertainty budget) for this two-step transformation will be illustrated in Section V-A

$$\begin{bmatrix} x \\ y \\ z \end{bmatrix}_{M1} = \mathbf{R}_0 \begin{bmatrix} x \\ y \\ z \end{bmatrix}_{M} \tag{3a}$$

$$\begin{bmatrix} x \\ y \\ z \end{bmatrix}_{W} = k \begin{bmatrix} 1 & \alpha' & -\beta' \\ -\alpha' & 1 & \gamma' \\ \beta' & -\gamma' & 1 \end{bmatrix} \begin{bmatrix} x \\ y \\ z \end{bmatrix}_{M1} + \begin{bmatrix} \Delta x \\ \Delta y \\ \Delta z \end{bmatrix} \tag{3b}$$

where the subscript $M1$ means the points in intermediate coordinate frame $\{M1\}$. $\mathbf{R}_0$ is the rotation matrix from $\{M\}$ to $\{M1\}$. α', β', and γ' are the rotation angles between $\{M1\}$ and $\{W\}$.

Reorganize (3b) as $\mathbf{B} = \mathbf{AX}$

$$\underbrace{\begin{bmatrix} x \\ y \\ z \end{bmatrix}_{W}}_{\mathbf{B}} = \underbrace{\begin{bmatrix} 1 & 0 & 0 & 0 & -z & y & x \\ 0 & 1 & 0 & z & 0 & -x & y \\ 0 & 0 & 1 & -y & x & 0 & z \end{bmatrix}_{M1}}_{\mathbf{A}} \underbrace{\begin{bmatrix} \Delta x \\ \Delta y \\ \Delta z \\ k\gamma' \\ k\beta' \\ k\alpha' \\ k \end{bmatrix}}_{\mathbf{x}}. \tag{4}$$

Assume n pairs of common points ($n > 3$) are measured, the complete equation is

$$\underbrace{\begin{bmatrix} x_1 \\ y_1 \\ z_1 \\ \vdots \\ x_n \\ y_n \\ z_n \end{bmatrix}_{W}}_{\mathbf{B}} = \underbrace{\begin{bmatrix} 1 & 0 & 0 & 0 & -z_1 & y_1 & x_1 \\ 0 & 1 & 0 & z_1 & 0 & -x_1 & y_1 \\ 0 & 0 & 1 & -y_1 & x_1 & 0 & z_1 \\ & & & \vdots & & & \\ 1 & 0 & 0 & 0 & -z_n & y_n & x_n \\ 0 & 1 & 0 & z_n & 0 & -x_n & y_n \\ 0 & 0 & 1 & -y_n & x_n & 0 & z_n \end{bmatrix}_{M1}}_{\mathbf{A}} \underbrace{\begin{bmatrix} \Delta x \\ \Delta y \\ \Delta z \\ k\gamma' \\ k\beta' \\ k\alpha' \\ k \end{bmatrix}}_{\mathbf{x}}. \tag{5}$$

III. Weighted Total Least Squares Adjustment and Weight Calculation

For (5), measurement errors exist in each common point in each coordinate frame such that both the vector $\mathbf{B}$ and matrix $\mathbf{A}$ include unknown errors. Therefore, (5) is an errors-in-variables (EIV) model, and its solving approach must treat vector $\mathbf{B}$ and matrix $\mathbf{A}$ symmetrically. Obviously, least squares adjustment is not feasible, since it assumes that the matrix $\mathbf{A}$ is error free. Besides, the approach must consider the uncertainty ellipsoid for each common point due to different error characteristics of different instruments. WTLS adjustment aims at estimating the vector $\mathbf{X}$ in EIV models and easily applies weights to subequations [16]–[19]. Moreover, WTLS adjustment provides an explicit formula to express the uncertainty of vector $\mathbf{X}$ so that calculation is simplified effectively. Therefore, WTLS adjustment is adopted in this paper.

A. Weighted Total Least Squares Adjustment Method

The WTLS adjustment is conceptually symbolized as

$$\mathbf{B} - \mathbf{e_B} = (\mathbf{A} - \mathbf{E_A})\,\mathbf{X} \tag{6}$$

where $\mathbf{B}$ is an observation vector affected by a random vector $\mathbf{e_B}$, and $\mathbf{A}$ is a coefficient matrix with full column rank affected by a random matrix $\mathbf{E_A}$. $\mathbf{X}$ is the unknown parameter vector. The stochastic properties of the vectors $\mathbf{e_B}$ and $\mathbf{e_A}$ are characterized by

$$\begin{bmatrix} \mathbf{e_B} \\ \mathbf{e_A} \end{bmatrix} \sim \left(\begin{bmatrix} 0 \\ 0 \end{bmatrix} \ \begin{bmatrix} \mathbf{Q_B} & 0 \\ 0 & \mathbf{Q_A} \end{bmatrix} \right) \tag{7}$$

where $\mathbf{e_A} = \mathrm{vec}(\mathbf{E_A})$, the symbol vec denotes the operator that converts a matrix to a column vector by stacking one column of this matrix underneath the previous one. $\mathbf{Q_B}$ and $\mathbf{Q_A}$ are the covariance matrices of $\mathbf{e_B}$ and $\mathbf{e_A}$, respectively.

The target function of solving the WTLS model is

$$\arg\min\left(\mathbf{e_B}^T\mathbf{Q_B}^{-1}\mathbf{e_B} + \mathbf{e_A}^T\mathbf{Q_A}^{-1}\mathbf{e_A}\right), \ \text{subject to (6).} \tag{8}$$

Several algorithms have been developed to solve the WTLS problem [18], [19]. Here, an iterative method proposed in [19] is adopted, because there are no demands on the structure of the covariance matrix $\mathbf{Q_A}$. Then, not only is the vector $\mathbf{X}$ estimated but also its covariance matrix, $\mathbf{D}_{\hat{X}}$, is solved

$$\mathbf{D}_{\hat{X}} = \left(\tilde{A}^T\mathbf{Q_L}^{-1}\tilde{A}\right)^{-1} \tag{9}$$

where $\mathbf{Q_L} = \mathbf{Q_B} + (\mathbf{X}^T \otimes \mathbf{I}_{3n})\mathbf{Q_A}(\mathbf{X} \otimes \mathbf{I}_{3n})$, $\tilde{\mathbf{A}} = \mathbf{A} - \tilde{E}_{\mathbf{A}}$, $\tilde{E}_{\mathbf{A}}$ is the predicted residual matrix, $\mathbf{I}_{3n}$ is a $3n \times 3n$ unit matrix, and $\otimes$ denotes the Kronecher–Zehfuss product of matrices, defined by $\mathbf{M} \otimes \mathbf{N} = [m_{ij} \cdot \mathbf{N}]$ for $\mathbf{M} = [m_{ij}]$.

Covariance matrix $\mathbf{D}_{\hat{X}}$ means the uncertainties of the seven transformation parameters, and it will be used to assess world-frame point's transformation uncertainty in Section IV.

B. Weighting by Measurement Uncertainty

Matrices $\mathbf{Q_B}$ and $\mathbf{Q_A}$ are the covariance matrices of vectors $\mathbf{e_B}$ and $\mathbf{e_A}$, respectively; thus, they consist of the measurement uncertainties of the common points in $\{W\}$ and $\{M1\}$.

Here, point uncertainty is represented by covariance matrix, and

$$\mathbf{Q_P} = \begin{bmatrix} \sigma_x^2 & \sigma_{xy} & \sigma_{xz} \\ \sigma_{yx} & \sigma_y^2 & \sigma_{yz} \\ \sigma_{zx} & \sigma_{zy} & \sigma_z^2 \end{bmatrix}. \tag{10}$$

Usually, a point's measurement uncertainty results from the uncertainties in the native sensor values and the conversion model of the measuring instrument. Take a laser tracker, for example. When measuring a point, a laser tracker provides a distance value (l) and two angle values (horizontal angle θ and vertical angle φ). In addition, manufacturers state the interferometer (or absolute) distance uncertainty (σ_l) and the angle uncertainty (σ_θ and σ_φ) in its specifications, as shown in Table I in Section V. Then the distance and angles are converted to the point coordinates

$$\begin{cases} x = l \sin\varphi \cos\theta \\ y = l \sin\varphi \sin\theta \\ z = l \cos\varphi. \end{cases} \tag{11}$$

During the conversion, uncertainty propagates from the native sensor values to point coordinates. In other words, according to the covariance propagation law, point's covariance matrix ($\mathbf{Q_P}$) is derived from the covariance matrix of the sensor values as follows:

$$\mathbf{Q_P} = \mathbf{J}\mathbf{Q}_0\mathbf{J}^T = \mathbf{J}\ \mathrm{Diag}\left(\sigma_l^2\ \sigma_\theta^2\ \sigma_\varphi^2\right)\mathbf{J}^T \tag{12}$$

where $\mathbf{Q}_0 = \mathrm{Diag}(\sigma_l^2\ \sigma_\theta^2\ \sigma_\varphi^2)$ is the covariance matrix of the sensor values and consist of the distance uncertainty and the angle uncertainties, and $\mathbf{J}$ is the Jacobian matrix of (11).

According to vector $\mathbf{B}$, matrix $\mathbf{Q_B}$ is a block diagonal matrix with diagonal of covariance matrix of each common point in {W}, assuming coordinates between different points are uncorrelated and

$$\mathbf{Q_B} = \mathrm{Diag}\left(\mathbf{Q}_{\mathbf{P}_1^W}\ \mathbf{Q}_{\mathbf{P}_2^W}\ \cdots\ \mathbf{Q}_{\mathbf{P}_n^W}\right) \tag{13}$$

where $\mathbf{Q}_{\mathbf{P}_i^W}$, $i = 1, 2, \ldots, n$ is the covariance matrix of common point $\mathbf{P}_i$ in $\{W\}$.

Similarly, matrix $\mathbf{Q_A}$ is filled with variances and covariance of common points in $\{M1\}$ according to vec($\mathbf{A}$). Since the points in {M1} are rigid rotated from $\{M\}$ by $\mathbf{R}_0$ and no addition uncertainties are involved during this transformation, the covariance matrix $\mathbf{Q}_{\mathbf{P}^{M1}}$ is derived from the matrix $\mathbf{Q}_{\mathbf{P}^M}$ with a similarity transformation [20]

$$\mathbf{Q}_{\mathbf{P}^{M1}} = \mathbf{R}_0\mathbf{Q}_{\mathbf{P}^M}\mathbf{R}_0^T. \tag{14}$$

IV. World-Frame Point's Transformation Uncertainty and Its Influencing Factors

After calculating the uncertainties of the transformation parameters from $\{M1\}$ to $\{W\}$, their effects on the final measurement results will be analyzed. First, a general formula is derived, which is for the transformation uncertainty of any point in $\{W\}$ transformed by the estimated transformation parameters. Then the distribution of the transformation uncertainty is simulated. Finally, the factors influencing the transformation uncertainty are analyzed.

A. World-Frame Point's Transformation Uncertainty

Let $\mathbf{P}^M = [\,x^M\ y^M\ z^M\,]^T$ be the coordinate vector of an arbitrary measured point in $\{M\}$ and $\mathbf{P}^W = [\,x^W\ y^W\ z^W\,]^T$ be the same point viewed from $\{W\}$. Then the relationship between two vectors $\mathbf{P}^M$ and $\mathbf{P}^W$ can be expressed as a function of 10 parameters

$$\begin{aligned} \begin{bmatrix} x^W \\ y^W \\ z^W \end{bmatrix} &= \begin{bmatrix} k & k\alpha' & -k\beta' \\ -k\alpha' & k & k\gamma' \\ k\beta' & -k\gamma' & k \end{bmatrix} \mathbf{R}_0 \begin{bmatrix} x^M \\ y^M \\ z^M \end{bmatrix} + \begin{bmatrix} \Delta x \\ \Delta y \\ \Delta z \end{bmatrix} \\ &= f(\mathbf{X}_0) \end{aligned} \tag{15}$$

where $\mathbf{X}_0 = [x^M\ y^M\ z^M\ \Delta x\ \Delta y\ \Delta z\ k\gamma'\ k\beta'\ k\alpha'\ k]^T$.

Since no addition uncertainties are involved during the rigid rotation $\mathbf{R}_0$, the covariance matrix of $\mathbf{P}^W$ can be computed by the covariance propagation law

$$\mathbf{Q}_{\mathbf{P}^W} = \mathbf{D}\mathrm{f}(\mathbf{X}_0)\mathbf{Q}_{\mathbf{X}_0}\mathbf{D}\mathrm{f}(\mathbf{X}_0)^T \tag{16}$$

where $\mathbf{Q}_{\mathbf{X}_0}$ is the covariance matrix of vector $\mathbf{X}_0$, which is composed of the covariance among the transformation parameters and that of $\mathbf{P}^M$, and

$$\mathbf{Q}_{\mathbf{X}_0} = \begin{bmatrix} \mathbf{Q}_{\mathbf{P}^M} & 0 \\ 0 & \mathbf{D}_{\hat{X}} \end{bmatrix}. \tag{17}$$

Note that the off-diagonal terms are all zeroes in the above matrix. The underlying assumption here is that transformation and measurement are two separate activities. $\mathbf{D}\mathrm{f}(\mathbf{X}_0)$ in (16) is the Jacobian matrix and is expressed as

$$\mathbf{D}\mathrm{f}\ (\mathbf{X}_0) = [\mathbf{R}'\mathbf{R}_0 \quad \mathbf{A_P}] \tag{18}$$

where

$$\mathbf{R}' = \begin{bmatrix} k & k\alpha' & -k\beta' \\ -k\alpha' & k & k\gamma' \\ k\beta' & -k\gamma' & k \end{bmatrix}$$

and

$$\mathbf{A_P} = \begin{bmatrix} 1 & 0 & 0 & 0 & -z_{\mathbf{P}} & y_{\mathbf{P}} & x_{\mathbf{P}} \\ 0 & 1 & 0 & z_{\mathbf{P}} & 0 & -x_{\mathbf{P}} & y_{\mathbf{P}} \\ 0 & 0 & 1 & -y_{\mathbf{P}} & x_{\mathbf{P}} & 0 & z_{\mathbf{P}} \end{bmatrix}_{M1}.$$

Therefore

$$\begin{aligned} \mathbf{Q}_{\mathbf{P}^W} &= [\mathbf{R}'\mathbf{R}_0 \quad \mathbf{A_P}] \begin{bmatrix} \mathbf{Q}_{\mathbf{P}^M} & 0 \\ 0 & \mathbf{D}_{\hat{X}} \end{bmatrix} \begin{bmatrix} \mathbf{R}_0{}^T\mathbf{R}'^T \\ \mathbf{A}_{\mathbf{P}}^T \end{bmatrix} \\ &= \mathbf{R}'\mathbf{R}_0\mathbf{Q}_{\mathbf{P}^M}\mathbf{R}_0^T\mathbf{R}'^T + \mathbf{A_P}\mathbf{D}_{\hat{X}}\mathbf{A}_{\mathbf{P}}^T. \end{aligned} \tag{19}$$

Covariance matrix $\mathbf{Q}_{\mathbf{P}^W}$ represents the uncertainty ellipsoid of world-frame point's transformation uncertainty.

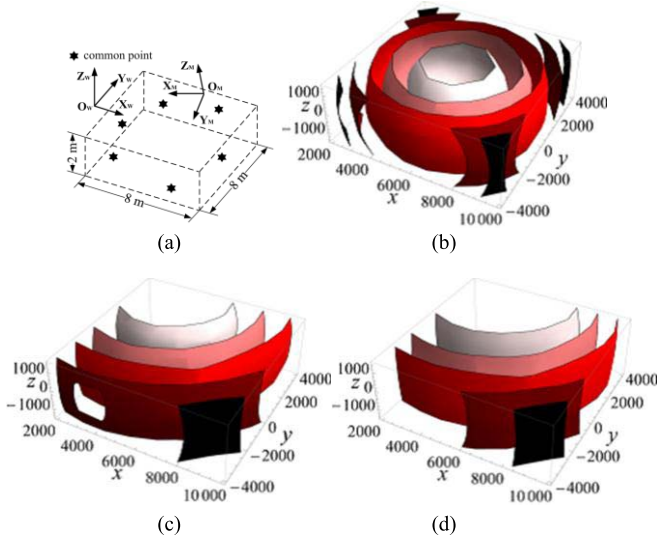

Fig. 1. Distribution of the overall uncertainty $(1-\sigma)$ of the transformed points. (a) Configuration of 3-D coordinate transformation. (b) Error model with independent, isotropic, and homogeneous distribution. (c) Laser-tracker model. (d) Double-theodolite mode.

Its eigenvectors give the directions of the principal axes of the uncertainty ellipsoid, and its eigenvalues give the variances along these principal axes

$$U_{\mathbf{P}W} = \sqrt{\text{trace}(\mathbf{Q}_{\mathbf{P}W})} = \sqrt{\text{trace}\left(\mathbf{R}'\mathbf{R}_0\mathbf{Q}_{\mathbf{P}M}\mathbf{R}_0^T\mathbf{R}'^T\right) + \text{trace}\left(\mathbf{A}_{\mathbf{P}}\mathbf{D}_{\hat{X}}\mathbf{A}_{\mathbf{P}}^T\right)} \tag{20}$$

where $U_{\mathbf{P}W}$ is a numerical representation of world-frame point's transformation uncertainty and means the overall uncertainty of this point.

B. Spatial Distribution of World-Frame Point's Transformation Uncertainty

Both $\mathbf{Q}_{\mathbf{P}W}$ and $U_{\mathbf{P}W}$ are broken into two parts. The first term $\mathbf{R}'\mathbf{R}_0\mathbf{Q}_{\mathbf{P}M}\mathbf{R}_0^T\mathbf{R}'^T$ is an orthogonal transformation of the covariance matrix $\mathbf{Q}_{\mathbf{P}M}$, so its trace is equal to the trace of $\mathbf{Q}_{\mathbf{P}M}$. The second term $\mathbf{A}_{\mathbf{P}}\mathbf{D}_{\hat{\mathbf{X}}}\mathbf{A}_{\mathbf{P}}^T$ or its trace depends not only on the covariance among the transformation parameters but also on the coordinates of the transformed point. In other words, the transformation uncertainty level in the whole measurement volume is not homogeneous. Here, three simulated functional images of the overall uncertainty $U_{\mathbf{P}W}$ with the same configuration and different error models are shown in Fig. 1: Fig. 1(a) shows the configurations of world frame O_W-$X_WY_WZ_W$ and measuring frame O_M-$X_MY_MZ_M$; Fig. 1(b)–(d) shows the spatial distributions of the overall uncertainty $(1-\sigma)$ with different measurement error models; Fig. 1(b) assumes the measurement error in each coordinate frame has an independent, isotropic, and homogeneous distribution; Fig. 1(c) assumes that both coordinate frames are laser tracker systems; Fig. 1(d) assumes the measuring coordinate frame is a double-theodolite system; and in Fig. 1(b)–(d), points in the same surface have the same overall uncertainty and darker color of the surface means a higher uncertainty.

Fig. 1 shows that the distribution of the transformation uncertainty is a group of concentric ellipsoids; the center point is with the minimum overall uncertainty and moving a point farther from the center increases its uncertainty.

Equations (19) and (20), and Fig. 1 all implicate that some criteria to choose the positions in the measurement volume are necessary to minimize the transformation uncertainty.

C. Factors Influencing a World-Frame Point's Transformation Uncertainty

The two parts in (19) and (20) indicate that if the transformation matrix is perfect, the measurement uncertainty of the transformed point in $\{M\}$ is the only error source. However, since uncertainties in the estimation of the transformation parameters are inevitable, the second part cannot be ignored. The factors influencing transformation uncertainty will now be analyzed, and some strategies for minimizing the uncertainty will be presented.

First, the measurement uncertainty of the transformed point in $\{M\}$ is caused by the measurement activity. Thus, its magnitude cannot be minimized during coordinate transformation while its orientation is changed. This section assumes that the measurement uncertainty of each transformed point is $\mathbf{Q}_{\mathbf{P}M} = \sigma^2\mathbf{I}_{3n}$, where $\sigma = 0.02$ mm.

Second, in terms of optimization, three common points are required to solve (5), and more common points result in more redundant constraints. Hence, it is obvious that the transformation uncertainty decreases as more common points are added. In view of the workload and cost for on-site measurement tasks, 6–10 common points are recommended in practical application.

Third, (9) shows that the covariance matrix of the transformation parameters $\mathbf{D}_{\hat{\mathbf{X}}}$ is determined by the measurement uncertainties and coordinates (layout) of common points. These two aspects will be analyzed separately in the following.

1) Impact of Measurement Uncertainties of Common Points: This section uses the uncertainties in the x-axis of common points as an example to illustrate the impact of the measurement uncertainty of common points on the transformation uncertainty; the conclusion can be generalized to the uncertainty in any direction of the common points.

A 3-D coordinate transformation is simulated with six common points arranged at random in a 10 m × 10 m × 4-m measurement volume, and a sampling grid of 21 × 21 × 21 points are set as the test points. The measurement uncertainty of each common point is assumed to be $\mathbf{Q}_{\mathbf{P}} = \text{Diag}(\sigma_x^2\ \sigma_y^2\ \sigma_z^2)$. During the simulation, σ_x is varied from 0 to 0.2 mm, while σ_y and σ_z are 0.02 mm. The graphs in Fig. 2 show the mean values $(1-\sigma)$ of the overall uncertainties and the x-, y-, and z-axis uncertainty components of test points: Fig. 2(a) shows the results with uncertainties of the world-frame common points varied and Fig. 2(b) shows those with uncertainties of the measuring-frame common points varied.

From these graphs, we observe the following.

1) Increasing the x-axis uncertainty components of common points in $\{W\}$ only increases the overall uncertainty

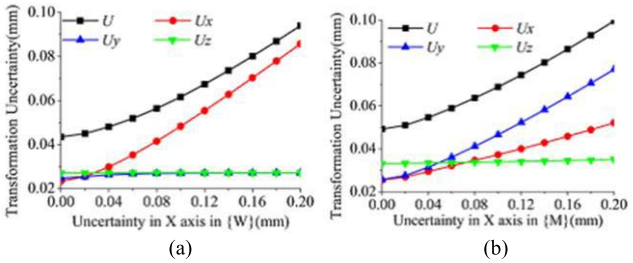

Fig. 2. Transformation uncertainty $(1-\sigma)$ with uncertainties of common points varied. (a) Variation of x uncertainty component in $\{W\}$. (b) Variation of x uncertainty component in $\{M\}$.

and the x-axis uncertainty component of the test point significantly, with little impact on the y- and z-axis components of the transformation uncertainty.

2) Increasing the x-axis uncertainty component of common points in $\{M\}$ increases the overall uncertainty as well as the x-, y-, and z-axis uncertainty components of the test point. In addition, the proportion of one component in the overall uncertainty is determined by the rotation between $\{M\}$ and $\{W\}$.
3) The measurement uncertainties of common points in both $\{W\}$ and $\{M\}$ have the same impact on the magnitude of the overall uncertainty.

Hence, decreasing common points' uncertainties is an efficient way to minimize transformation uncertainty. In large-scale metrology, this can be achieved using more accurate instruments or rearranging the relative positions of common points and the instrument. If the transformation uncertainty in a specific direction must be limited, decreasing the uncertainty component in that direction of common points in $\{W\}$ is recommended.

2) Impact of Common-Point Layout: This section uses several 2-D layouts in the xoy plane as an example to illustrate the impact of the common-point layout; the conclusion can be generalized to 3-D layouts. In each layout, six common points and two groups of test points x and y are arranged, assuming that all common points have the same measurement uncertainties, $\mathbf{Q_P} = \sigma^2\mathbf{I}_{3n}$, where $\sigma = 0.02$ mm.

First, four specific O-layouts are compared, three with uniform distributions and diameters of 10 m [Fig. 3(a)], 5 m [Fig. 3(b)], 14 m [Fig. 3(c)], respectively, and one with a nonuniform distribution and a 10-m diameter [Fig. 3(d)], as shown in Fig. 3. Fig. 4 shows the overall uncertainties $(1-\sigma)$ of test points in Fig. 3(a)–(d). From the figures, the following facts are clear.

1) The layouts that fully surround the measurement area are optimal. If not, the transformation uncertainty increases rapidly, especially for the test points outside the common-point circle.
2) On the premise of 1), expanding the area encircled by the common points produces a little reduction in transformation uncertainty.
3) Whether the distribution is uniform or not has little effect on the mean transformation uncertainty.

Second, two C-layouts with common points placed on a 10-m diameter semicircle along test points x and y,

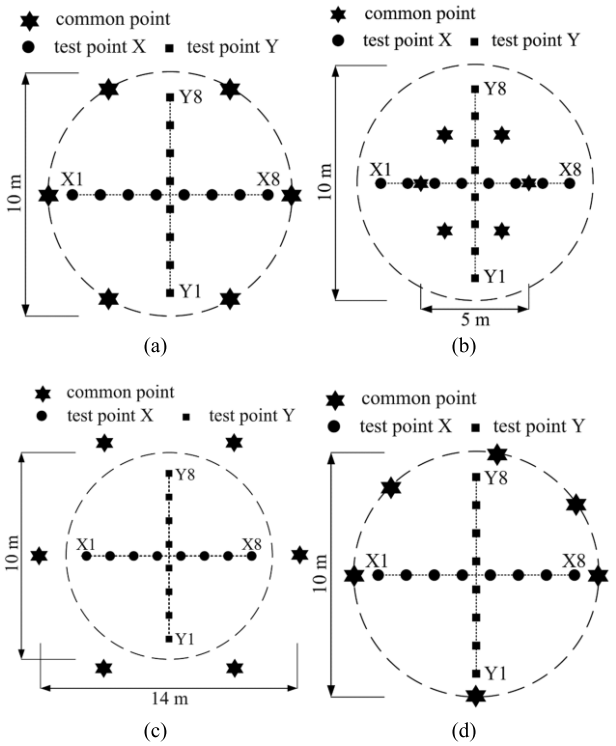

Fig. 3. Illustration for O-layouts of common points. (a) Uniform O-layout with 10-m diameter. (b) Uniform O-layout with 5-m diameter. (c) Uniform O-layout with 14-m diameter. (d) Nonuniform O-layout with 10-m diameter.

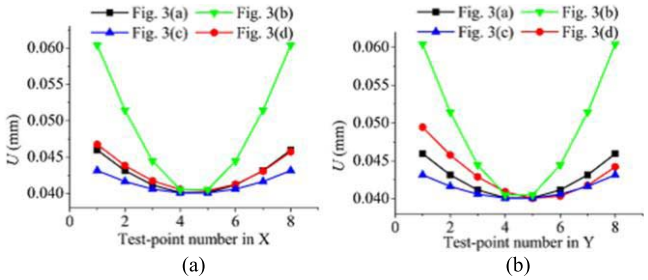

Fig. 4. Comparison of the transformation uncertainties $(1-\sigma)$ in four O-layouts. (a) Overall uncertainties of the test points x. (b) Overall uncertainties of the test points y.

respectively, are compared, as shown in Fig. 5, with the results summarized in Fig. 6. It is obvious that compared with the test points perpendicular to the direction of common points, the uncertainties of the test points along the direction of common points is decreased more by the C-shaped layout.

Third, the x, y, and z uncertainty components of test points x in Figs. 3(a) and 5(a) and (b) are compared in Fig. 7. From the figures, the following facts are obvious.

1) In each layout, the x-axis uncertainty component is equal to the y-axis component.
2) The x- and y-axis uncertainty components are decreased more than the z-axis component.
3) Compared with the C-shaped layout, the O-shaped layout minimizes the z-axis uncertainty component effectively.

In summary, the common points must encircle the entire measurement volume, and as the encircled area expands, the

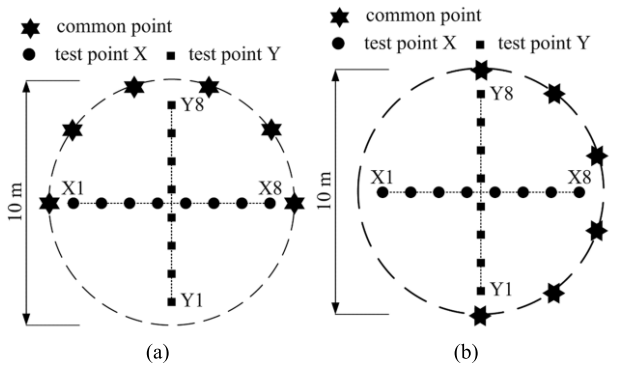

Fig. 5. Illustration for C-layouts of common points. (a) C-layout along test points x. (b) C-layout along test points y.

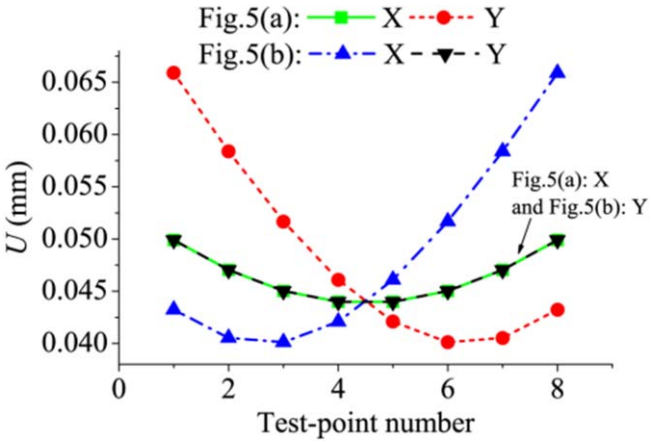

Fig. 6. Comparison of transformation uncertainties $(1-\sigma)$ in two C-layouts.

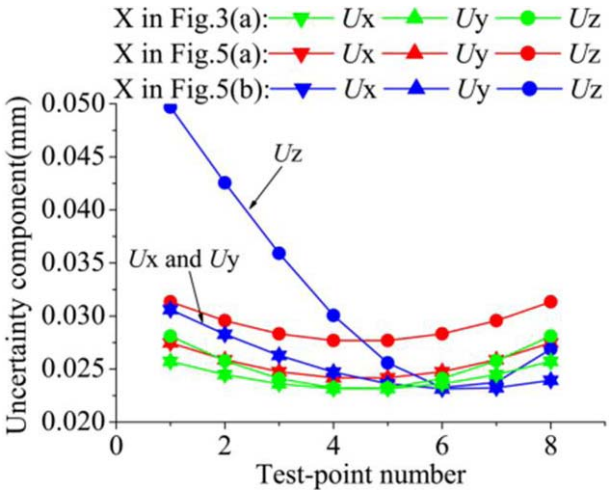

Fig. 7. Comparison of uncertainty components of test points x.

uncertainty decreases. If this is infeasible due to obstructions, the C-shaped layout along the direction of transformed points is recommended. To limit the uncertainty in a specific direction, a 2-D layout parallel to this direction is adequate.

Owing to the inhomogeneous distribution of the measurement uncertainty of nonorthogonal coordinate measurement systems in measurement volume, expanding the area encircled by common points frequently results in an increase in the measurement uncertainties of those points. Hence in practical application, a compromise must be made between decreasing the uncertainties of common points and expanding the volume they encircled.

TABLE I
UNCERTAINTY PARAMETERS (IN MPE) OF A LEICA AT901-LR LASER TRACKER

Component	Uncertainty
Interferometer Accuracy	0.5 μm/m
Absolute Distance Meters accuracy	± 10 μm
Angle accuracy, full range	± 15 μm + 6 μm/m

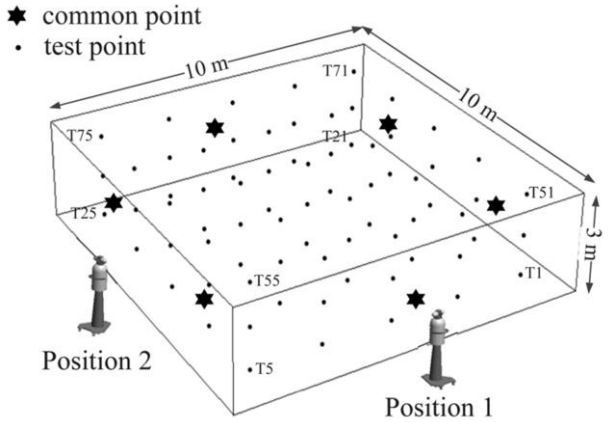

Fig. 8. Setup of Experiment 1.

V. EXPERIMENTAL VERIFICATION

To verify the proposed 3-D coordinate transformation uncertainty estimation approach (analytical approach) and the influencing factors, two experiments were conducted with a Leica AT901-LR laser tracker. The uncertainty parameters [in maximum permissible error (MPE)] of the laser tracker [21], [22] are listed in Table I. Experiments 1 and 2 were conducted to validate the analytical approach and to illustrate the strategies recommended in Section IV-C, respectively.

A. Verification of Analytical Approach

Experiment 1 was conducted in a 10 m × 10 m × 3 m volume, with the setup shown in Fig. 8. Six common points were arranged surrounding 75 test points. The two tracker positions were approximately 1 m from the volume and 8.5 m apart. The test results for 3-D coordinate transformation were analyzed using the analytical approach and the MC simulation [23]. For the MC simulation, the sample size was 10 000 and transformation model was the quaternion model [24].

For the transformation uncertainty, the components of the analytical approach and the MC simulation are differenced and plotted in Fig. 9. It is seen that the values obtained using the analytical approach are less than those obtained using the MC simulation. The mean difference $(1-\sigma)$ is

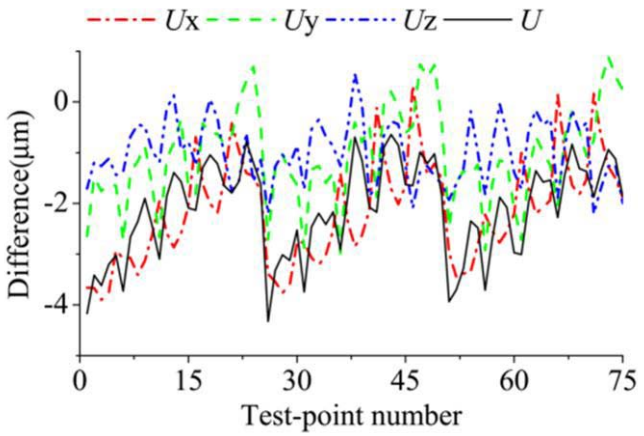

Fig. 9. Analytical approach minus the MC simulation.

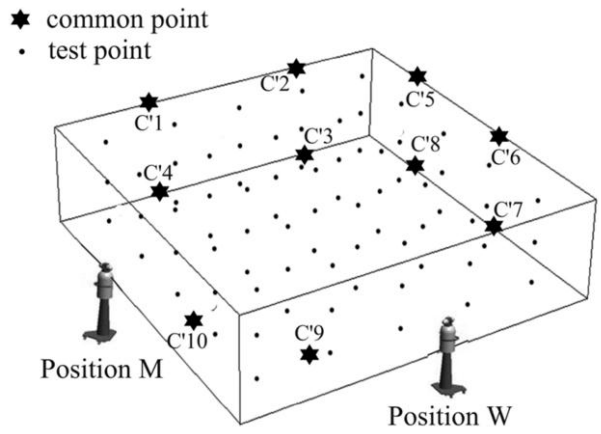

Fig. 10. Configuration of Experiment 2.

about 2 μm and the maximum is less than 4.5 μm. These discrepancies are caused primarily by three factors. First, (8) takes full account of common points' uncertainties, while the quaternion model does not. This is one advantage of the analytical approach. Next, two-step transformation is adopted between $\{M\}$ and $\{W\}$, in which the rotation matrix between $\{M1\}$ and $\{W\}$ is linearized by small angles. Finally, the higher order terms are neglected in the covariance propagation law. To verify these discrepancies, the test results were analyzed again, assuming that the measurement uncertainties of the individual points are the same, in other words, neglecting the first factor. Then the mean difference is reduced to 1 μm, with the maximum less than 2 μm. This means that compared with the quaternion model, the WTLS-based model can minimize the transformation uncertainty and that the errors introduced by both the two-step transformation and the covariance propagation law are small enough to be accepted under normal instrument operating conditions.

Another distinction between the analytical approach and the MC simulation is the computational expense. The two approaches ran in MATLAB R2009a on a Core-i5 2.8-GHz machine. The analytical approach took less than 0.2 s and occupied less than 0.14 MB, while the MC simulation executed in 2 s and occupied 72 MB. It is clear that the MC simulation is computationally more expensive than the analytical approach, and this expense grows exponentially as the number of measured points increases.

B. Verification of Influencing Factors

In the common-point layout in Experiment 1, the maximum transformation uncertainty is greater than 0.095 mm, and the uncertainty introduced by 3-D coordinate transformation [part 2 in (20), introduced uncertainty] is approximately 0.06 mm, while the measurement uncertainties of test points [part 1 in (20)] are less than 0.075 mm. In Experiment 2, to illustrate the strategies recommended in Section IV-C, the measurement specification assumes that the introduced uncertainty at each test point is within 0.04 mm and common points are rearranged. The setup is shown in Fig. 10, and the introduced uncertainties in Experiments 1 and 2 are compared in Fig. 11.

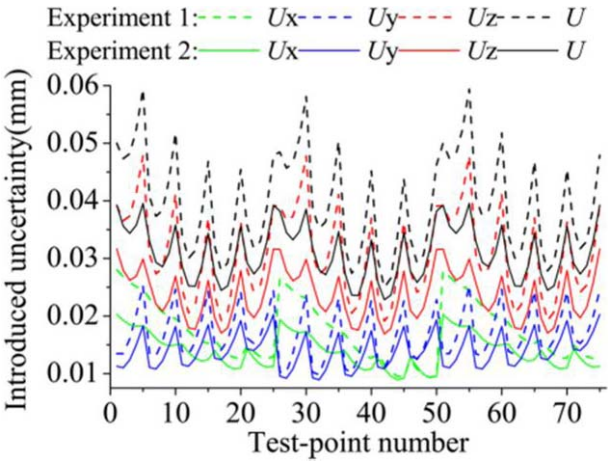

Fig. 11. Comparison of the introduced uncertainties $(1-\sigma)$ at test points.

For the laser tracker, the distance measurement value is much more accurate than the angular measurement value. Thus, a point's measurement uncertainty has a flattened shape perpendicular to the radial. In addition, owing to the spherical coordinates model, moving a point farther from the instrument increases its uncertainty.

The graphs in Fig. 11 show that in Experiment 1, the test points where the introduced uncertainties exceed 0.04 mm are all near common points C2–C4, and the z-axis uncertainty component accounts for a large proportion. This is because the uncertainties of common points C2–C4 are greater than those of other common points, and the 2-D common-point layout makes it difficult to reduce the introduced uncertainty in the z-axis. Therefore in Fig. 10, points C2–C4 are replaced with two O-shaped layouts of common points C′1–C′4 and C′5–C′8 to minimize the introduced uncertainty, especially the z-axis component. Then to balance the accuracy and the workloads, the three points C1, C5, and C6 are reduced to the two points C′9 and C′10.

In addition, two other layouts are considered: an O-layout similar to that of Experiment 1 and a double-decker O-layout. In both layouts, at least 14 common points are required. Therefore, the layout in Fig. 10 meets the measurement specification

with the fewest workloads. This means that the strategies recommended in Section IV-C are helpful for minimizing transformation uncertainty and reducing measurement cost.

VI. Conclusion

The WTLS-based 3-D coordinate transformation uncertainty estimation approach was discussed in detail. This approach satisfies any rotation angle and uses information from the instruments' uncertainty characteristics fully. In addition, it has the advantages of simplification and less calculation. The MC simulation was used to validate this approach, resulting in the finding that the two-step transformation is justified for normal instrument operating conditions. The transformation uncertainty was found to depend on a point's position, and its distribution rule is a group of concentric ellipsoids. Through the simulation, the impacts of the measurement uncertainties and layout of common points on transformation uncertainty were analyzed in detail and some strategies on measurement configurations were recommended. The experimental results demonstrated that these strategies minimize transformation uncertainty and reduce measurement cost effectively. Hence, the proposed approach can be adapted easily to the uncertainty evaluation of 3-D coordinate transformation results in large-scale metrology, and the recommended strategies can optimize common-point layout, instrument type, and placement in the on-site measurement tasks efficiently.

References

[1] W. T. Estler, K. L. Edmundson, G. N. Peggs, and D. H. Parker, "Large-scale metrology—An update," *CIRP Ann.-Manuf. Technol.*, vol. 51, no. 2, pp. 587–609, 2002.

[2] P. G. Maropoulos, Y. Guo, J. Jamshidi, and B. Cai, "Large volume metrology process models: A framework for integrating measurement with assembly planning," *CIRP Ann.-Manuf. Technol.*, vol. 57, no. 1, pp. 477–480, 2008.

[3] J. M. Calkins, "Quantifying coordinate uncertainty fields in coupled spatial measurement systems," Ph.D. dissertation, Dept. Mech. Eng., Virginia Polytech. Inst., State Univ., Blacksburg, VA, USA, 2002.

[4] Z. Yan and C.-H. Menq, "Uncertainty analysis and variation reduction of three-dimensional coordinate metrology. Part 2: Uncertainty analysis," *Int. J. Mach. Tools Manuf.*, vol. 39, no. 8, pp. 1219–1238, 1999.

[5] C. Che and J. Ni, "A generic coordinate transformation uncertainty assessment approach and its application in machine vision metrology," *Int. J. Mach. Tools Manuf.*, vol. 38, nos. 10–11, pp. 1241–1256, 1998.

[6] T. Takatsuji, M. Goto, A. Kirita, T. Kurosawa, and Y. Tanimura, "The relationship between the measurement error and the arrangement of laser trackers in laser trilateration," *Meas. Sci. Technol.*, vol. 11, no. 5, pp. 477–483, 2000.

[7] J. E. Muelaner *et al.*, "Study of the uncertainty of angle measurement for a rotary-laser automatic theodolite (R-LAT)," *J. Eng. Math.*, vol. 223, no. 3, pp. 217–229, 2009.

[8] J. E. Muelaner, Z. Wang, O. Martin, J. Jamshidi, and P. G. Maropoulos, "Estimation of uncertainty in three-dimensional coordinate measurement by comparison with calibrated points," *Meas. Sci. Technol.*, vol. 21, no. 2, p. 025106, 2010.

[9] B. Hughes, A. Forbes, A. Lewis, W. Sun, D. Veal, and K. Nasr, "Laser tracker error determination using a network measurement," *Meas. Sci. Technol.*, vol. 22, no. 4, p. 045103, 2011.

[10] *Spatial Analyzer User Manual*, New River Kinematics, Virginia, USA, 2014. [Online]. Available: http://kinematics.com

[11] *Evaluation of Measurement Data—Guide to the Expression of Uncertainty in Measurement*, the Joint Commitee for Guides in Metrology, JCGM Standard 100:2008, Sep. 2014. [Online]. Available: http://www.iso.org/sites/JCGM/GUM-introduction.htm

[12] O. Faugeras, "Computing uncertainty," in *Three-Dimensional Computer Vision: A Geometric Viewpoint*. Cambridge, MA, USA: MIT Press, 1993, pp. 151–162.

[13] B. R. Harvey, "Transformation of 3D co-ordinates," *Austral. Surv.*, vol. 33, no. 2, pp. 105–125, 1986.

[14] H. S. Kutoglu, C. Mekik, and H. Akcin, "A comparison of two well known models for 7-parameter transformation," *Austral. Surv.*, vol. 47, no. 1, pp. 24–30, 2002.

[15] W. X. Zeng and B. Z. Tao, "Non-linear adjustment model of three-dimensional coordinate transformation," *Geomatics Inf. Sci. Wuhan Univ.*, vol. 28, no. 5, pp. 566–568, 2003.

[16] Y. A. Felus and B. Schaffrin, "Performing similarity transformations using the error-in-variables model," presented at the Amer. Soc. Photogrammetry Remote Sens. (ASPRS) Annu. Conf., Baltimore, MD, USA, Mar. 2005.

[17] I. Markovsky and S. Van Huffel, "Overview of total least-squares methods," *Signal Process.*, vol. 87, no. 10, pp. 2283–2302, 2007.

[18] B. Schaffrin and A. Wieser, "On weighted total least-squares adjustment for linear regression," *J. Geodesy*, vol. 82, no. 7, pp. 415–421, 2008.

[19] Y. Shen, B. Li, and Y. Chen, "An iterative solution of weighted total least-squares adjustment," *J. Geodesy*, vol. 85, no. 4, pp. 229–238, 2011.

[20] G. H. Golub and C. F. Van Loan, "Orthogonalization and least squares," in *Matrix Computations*, vol. 3. Baltimore, MD, USA: The Johns Hopkins Univ. Press, 1996, p. 311.

[21] *Leica Absolute Tracker AT901 & PCMM System Specs*, Hexagon Metrology, London, U.K., 2012. [Online]. Available: http://www.hexagonmetrology.com/

[22] *Leica Absolute Tracker AT901 ASME Specifications*, Leica Geosystems, Unterentfelden, Switzerland, 2008. [Online]. Available: http://metrology.leica-geosystems.com/

[23] C. E. Papadopoulos and H. Yeung, "Uncertainty estimation and Monte Carlo simulation method," *Flow Meas. Instrum.*, vol. 12, no. 4, pp. 291–298, 2001.

[24] D. W. Eggert, A. Lorusso, and R. B. Fisher, "Estimating 3-D rigid body transformations: A comparison of four major algorithms," *Mach. Vis. Appl.*, vol. 9, nos. 5–6, pp. 272–290, 1997.

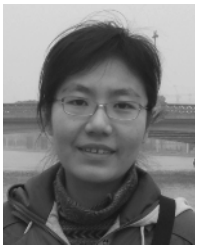

Yu Ren received the bachelor's degree from Tianjin University, Tianjin, China, in 2011, where she is currently pursuing the Ph.D. degree with the College of Precision Instrument and Opto-Electronics Engineering.

Her current research interests include laser and photoelectric measurement.

Jiarui Lin received the Ph.D. degree in precision instrument engineering from Tianjin University, Tianjin, China, in 2012.

He is currently a Lecturer with the College of Precision Instrument and Opto-Electronics Engineering, Tianjin University. His current research interests include laser and photoelectric measurement and large-scale precision metrology.

Jigui Zhu received the M.S. degree from the National University of Defense Technology, Changsha, China, in 1994, and the Ph.D. degree from Tianjin University, Tianjin, China, in 1997.

He is currently a Professor with the College of Precision Instrument and Opto-Electronics Engineering, Tianjin University. His current research interests include laser and photoelectric measurement, robot vision, and online vision inspection.

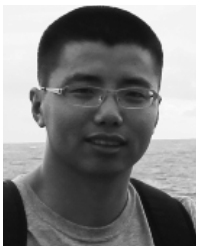

Bo Sun received the bachelor's and master's degrees from Tianjin University, Tianjin, China, in 2011 and 2014, respectively, where he is currently pursuing the Ph.D. degree with the College of Precision Instrument and Opto-Electronics Engineering.

His current research interests include laser and photoelectric measurement.

Shenghua Ye received the M.S. degree from Tianjin University, Tianjin, China, in 1962.

He is currently a Professor and Group Leader of the State Key Laboratory of Precision Measuring Technology and Instruments, Tianjin University. His current research interests include laser and photoelectric measurement.

Prof. Ye is a member of the Chinese Academy of Engineering.